



ELSEVIER

Journal of Non-Crystalline Solids 263&264 (2000) 213–227

JOURNAL OF  
NON-CRYSTALLINE SOLIDS

www.elsevier.com/locate/jnoncrystal

# Effects of OH content, water vapor pressure, and temperature on sub-critical crack growth in phosphate glass

T.I. Suratwala<sup>a,\*</sup>, R.A. Steele<sup>a</sup>, G.D. Wilke<sup>a</sup>, J.H. Campbell<sup>a</sup>, K. Takeuchi<sup>b</sup>

<sup>a</sup> Lawrence Livermore National Laboratory, P.O. Box 808, Livermore, CA 94551, USA

<sup>b</sup> Hoya Corporation USA, 3400 Edison Way, Fremont, CA 94538, USA

## Abstract

The effects of temperature and water vapor pressure on the rate of sub-critical crack growth in meta-phosphate laser glasses containing different OH concentrations (128 and 773 ppmw) are reported. The crack velocity was measured using the double-cleavage-drilled-compression method. When plotted as a function of stress intensity, the samples have the classic region I, II and III crack growth properties similar to that reported for silicate glasses. The glass containing the larger OH content has a 10-fold greater crack velocity in region I; crack velocities in region II are the nearly the same for both glasses. The crack velocities are analyzed using a chemical kinetic and mass-transport limited reaction rate model. At temperatures  $>150^{\circ}\text{C}$  and water vapor pressures  $>10$  mmHg, crack tip blunting is observed and the glass containing the larger OH content is more prone to blunting. © 2000 Published by Elsevier Science B.V. All rights reserved.

## 1. Introduction

Nd-doped metaphosphate glasses are the preferred gain medium for high-peak-power lasers used for fusion research mainly because they can store optical energy at greater densities than other glass-types and this energy can be efficiently extracted [1,2]. However, one problem with the use of phosphate glasses as laser ion hosts is that they have larger thermal expansion and lower fracture toughness than do, for example, silicates [3]. Consequently phosphates are more prone to fracture.

It is known that a crack can propagate from an existing flaw even at stresses less than that for

critical failure. This phenomenon is known as slow crack growth, stress corrosion cracking, or sub-critical crack growth [4–15]. The velocity of the fracture can vary by orders of magnitude, from  $<1$   $\mu\text{m}/\text{min}$  up to many meters per second. Consequently the time-to-failure for a given glass component can also vary by orders of magnitude. Because of their relatively poor mechanical properties, phosphate glasses are particularly susceptible to slow crack growth. However, despite the numerous studies on slow crack growth in silicate glasses [4–13], to our knowledge few studies have investigated this phenomenon in phosphate glasses [14,15]. Such information is of practical importance to the manufacture and use of phosphate glasses in mega-joule scale laser systems [16–18].

Crack growth has been hypothesized to occur by a stress-enhanced chemical reaction at the crack tip which for phosphate glass can be given by [14]

\* Corresponding author. Tel.: 1-925 422 1884; fax: 1-925 423 0792.

E-mail address: suratwala1@llnl.gov (T.I. Suratwala).



and/or



where M is an metal cation. In Eq. (1a) the  $\text{H}_2\text{O}$  reacts with the phosphorous–oxygen–phosphorous linkage at the crack tip and forms chain terminating hydroxyl groups; while in Eq. (1b) the  $\text{H}_2\text{O}$  reaction does not break up the P–O–P backbone, but separates links between chains. With both reactions crack propagation takes place.

In a previous paper [14], we report slow crack growth velocities in phosphate glass having an OH content <100 ppm. The measured crack growth velocities, when plotted as a function of stress intensity, have regions I, II and III velocities [4,14]. The data were analyzed using Wiederhorn's reaction rate model for slow crack growth [4]. This model includes a description of the  $\text{H}_2\text{O}$  reaction kinetics at the crack tip as well as  $\text{H}_2\text{O}$  mass transport to the reaction interface. By fitting this model to the data, a set of empirical parameters were developed that predicted slow crack growth over a range of temperatures, water vapor pressures, and stress intensities.

The work reported here expands the study of slow crack growth in phosphate glasses to include the effects of residual OH content in the glass. More specifically, the rate of crack growth as a function of stress intensity, temperature and water vapor pressure is reported in two glasses that have a six-fold difference in OH content. This difference is because during melting phosphate glasses readily react with water vapor in the ambient atmosphere producing chain terminating OH groups. The results of the present work are presented in several sections. First the data showing the region I, II and III slow crack growth are presented, and the region I and II data are fit using Wiederhorn's reaction rate model. The observed crack growth is compared with that reported for other glasses (phosphates and silicates). Next we discuss the effects of the hydroxyl content in the glass on the measured slow crack growth. Finally, the conditions that promote crack blunting are compared with predictions of models for slow crack propa-

gation. Also, we suggest that water condensation may occur at the crack tip under certain test conditions.

## 2. Experimental procedures

Two phosphate laser glasses, LHG-8L and LHG-8H were prepared containing hydroxyl group contents of about 130 and 770 ppmw; here we use the designations 'L' and 'H' to denote the low and high OH content of the glasses, respectively. The base glass used in this study is a commercial metaphosphate laser glass, LHG-8 (Hoya Corporation), having the molar composition:  $(55-60)\text{P}_2\text{O}_5-(8-12)\text{Al}_2\text{O}_3-(13-17)\text{K}_2\text{O}-(10-15)\text{BaO}-(0-2)\text{Nd}_2\text{O}_3$ .

The compositions are reported as ranges to account for variability due to doping and melting methods and to protect certain proprietary aspects of the composition [18]. There is little variation in glass properties over this range of compositions. For example, recently Campbell and Suratwala [3] have reported laser, optical and physical properties for a number of phosphate glasses having compositions that span the range given here and report that most properties vary by less than  $\pm 20\%$ .

The glasses used in this study were prepared using the melt procedures discussed elsewhere [18]. The hydroxyl content was varied by changing the degree of  $\text{O}_2$  bubbling (1-atm) through the glass during the melting phase at 1400 K [18]. The cast glasses were cooled at a rate <20 K/h from  $T_g$  to room temperature giving a residual stress birefringence <10 nm/cm (i.e., residual stress <0.5 MPa).

The hydroxyl content of the glass was determined from the infrared absorption of the –O–H stretching band at 3333 nm ( $3000\text{ cm}^{-1}$ ) [19]. The measured OH absorption coefficient at  $3000\text{ cm}^{-1}$  and some other properties for both LHG-8L and LHG-8H samples are shown in Table 1. To relate the OH absorption coefficient to the absolute OH concentration, the extinction coefficient must be known. However, reported extinction coefficients vary from 30 to 100 ppmw/ $\text{cm}^{-1}$  (from 70 to 230 l/mol cm) at  $3000\text{ cm}^{-1}$  [20]. An extinction coefficient of 30 ppmw/ $\text{cm}^{-1}$  ( $\approx 70\text{ l/mol cm}$ ) is assumed

Table 1  
Hydroxyl content and glass transition temperature for the LHG-8 glasses used in this study

Glass	Optical absorption at 3333 nm ( $\text{cm}^{-1}$ ) ( $\pm 4\%$ )	Implied OH content <sup>a</sup> (ppmw)	$T_g$ ( $^{\circ}\text{C}$ ) ( $\pm 5$ )
LHG-8L	4.2	128	472
LHG-8H	25.5	773	425

<sup>a</sup> Assumes 30 ppmw OH per  $\text{cm}^{-1}$  absorption at 3333 nm.

based on earlier work by Toratani [21] on phosphate laser glasses.

The slow crack growth velocities were measured by the double-cleavage-drilled-compression (DCDC) technique. A schematic of the experimental setup is shown in Fig. 1. The details of the experimental procedure are described elsewhere [14]. Briefly, the technique utilizes rectangular glass samples ( $75 \times 7.5 \times 6.5 \text{ mm}^3$ ) with a hole (1 mm radius) drilled in the center of the  $75 \times 7.5 \text{ mm}^2$  face. The samples were mounted in a mechanical testing machine (Instron 8562) within an environmentally controlled chamber. The applied compressive stress was typically 400–500 psi. The velocity of the cracks originating from the sample hole (which is under tension) was determined by monitoring the position of the crack front as a function of time using a cathetometer. The diffraction limited resolution of the cathetometer was about  $6 \times 10^{-5}$  rad which, for our experimental geometry, allows measurement of the crack front position to within  $\pm 10 \mu\text{m}$ . Crack velocities were measured for both glasses (LHG-8H and LHG-8L) at various temperatures ranging from  $25^{\circ}\text{C}$  to

$300^{\circ}\text{C}$  and ambient water vapor pressures from 2 to 92 mmHg. Each set of data for a single set of conditions represents the measurements from a single sample. The water vapor pressure was generated by bubbling  $\text{N}_2$  gas through water contained in a temperature-controlled water bath. Stress intensities,  $K_I$  ( $\text{MPa m}^{1/2}$ ), were calculated from the applied stress,  $\sigma$  (MPa), measured crack length,  $l$  (m) and hole radius,  $a$  (m), using the relationship developed by Michalske et al. [22]

$$K_I = \frac{\sigma\sqrt{a}}{1.595 + 0.353(l/a)}. \quad (2)$$

### 3. Results

Crack velocity measurements, when presented as plots of log velocity vs.  $K_I$ , typically have three distinct regions, I, II and III. These regions have been observed in a number of glasses [4,11,14,23]. All three of these regions are observed in LHG-8 phosphate glass at  $25^{\circ}\text{C}$  and 2 mmHg (see Fig. 2). Region I refers to the condition when crack growth is reaction-rate limited and has a linear relation between  $\log v$  and  $K_I$ . In other words, transport of  $\text{H}_2\text{O}$  to the crack tip is rapid enough that crack growth is limited only by the rate of reaction between  $\text{H}_2\text{O}$  and the P–O–P or P–O–M bond (Eq. (1)). For example, at  $25^{\circ}\text{C}$  and 2 mmHg  $\text{H}_2\text{O}$  vapor pressure, the crack velocity in LHG-8L samples is  $3.0 \pm 0.3 \times 10^{-7}$  m/s ( $0.3 \mu\text{m/s}$ ) at a  $K_I$  of 0.405  $\text{MPa m}^{1/2}$ . Increasing  $K_I$  to 0.420  $\text{MPa m}^{1/2}$  results in about an order-of-magnitude increase in the crack velocity to  $6.0 \pm 0.5 \times 10^{-6}$  m/s ( $6 \mu\text{m/s}$ ). This exponential dependence of crack velocity with  $K_I$  is seen in Fig. 2; it is commonly observed in other glasses, ceramics and even polymers [4,5,24–29].

In region II, the crack velocity is no longer reaction-rate-limited but instead becomes limited by

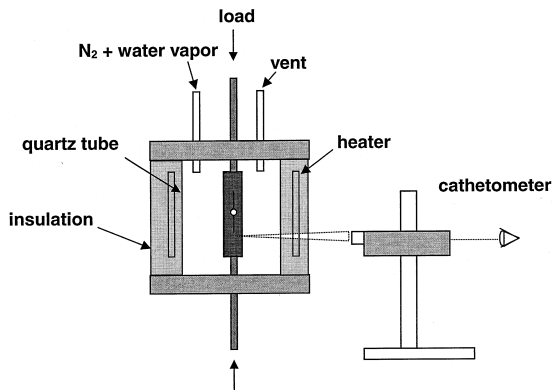


Fig. 1. Schematic of the experimental setup used to measure slow crack growth velocities using the DCDC method.

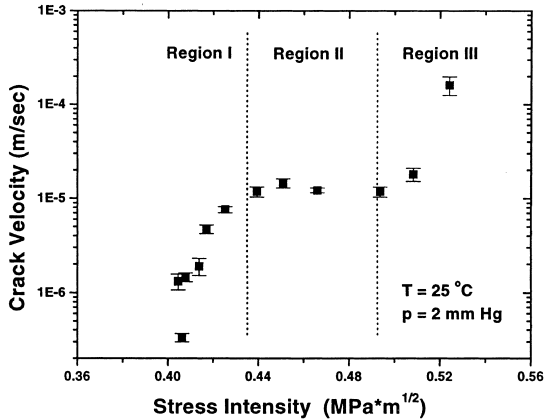


Fig. 2. Measured crack velocity ( $v$ ) in LHG-8L (a low OH content glass) as a function of stress intensity ( $K_I$ ) illustrating region I, II and III slow crack growth. The measurements were carried out at 25°C and a water vapor pressure of 2 mm Hg.

mass-transport (diffusion) of  $H_2O$  to the crack tip [6]. Consequently, region II is usually observed at smaller vapor pressures and lower temperatures where mass transport rates are slower. The measured crack velocities in region II remain nearly constant with increasing  $K_I$ .

Finally, in region III the crack velocity becomes independent of the chemical environment and is limited by the intrinsic toughness of the glass [6]. The on-set of region III, as indicated by an increase in velocity at the end of region II (see Fig. 2), typically occurs as  $K_I$  approaches the glass fracture toughness. The fracture toughness of LHG-8 samples has been measured by the chevron notch method [30] to be  $0.51 \text{ MPa m}^{1/2}$ ; notice in Fig. 2 that the onset of region III occurs just below this fracture toughness.

The measured slow crack velocities for LHG-8L glass at various temperatures and water vapor pressures are shown in Fig. 3. Crack velocities increase with both temperature (Fig. 3(a)) and water vapor pressure (Fig. 3(b)). In region I the crack velocity increases linearly with the  $H_2O$  vapor pressure and can be fit with an Arrhenius-type temperature dependence [4,5] with an activation energy of  $253 \pm 3 \text{ kJ/mol}$ .

The effect of the LHG-8 OH content on the slow crack growth velocities at different temperatures and water vapor pressures is shown in Fig. 4.

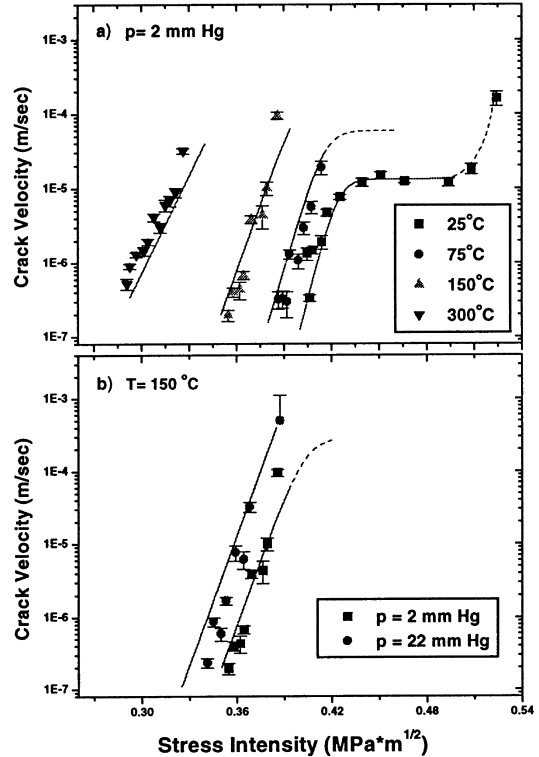


Fig. 3. Crack growth velocity ( $v$ ) in LHG-8L (a low OH content glass) as function of stress intensity ( $K_I$ ) at (a) various temperatures and (b) water vapor pressures. The points represent measured velocities and the curves represent model predictions using Eq. (7) and the model parameters listed in Table 2.

The crack velocities in the low OH content glass, LHG-8L, are indicated by the solid data points, and in the high OH content glass, LHG-8H, by the open data points. At equivalent stress intensities ( $K_I$ ), the larger OH content glass has faster crack velocities in both region I and III. Region II appears to be unaffected by the hydroxyl content of the glass (Fig. 4(a)).

## 4. Discussion

### 4.1. Chemical and mass-transport-limited reaction rate model

As described in Section 1, the proposed mechanism of slow crack growth in phosphate glass is

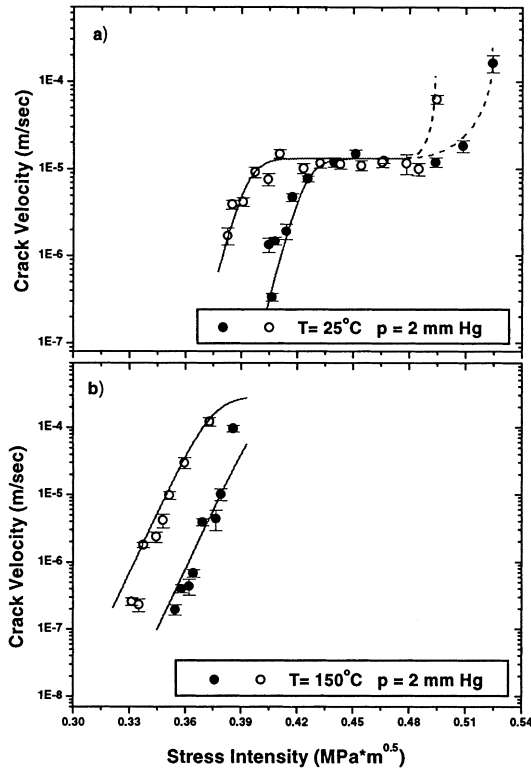


Fig. 4. Sub-critical crack growth velocities ( $v$ ) as a function of stress intensity ( $K_I$ ) for LHG-8 glasses containing low and high OH contents, i.e. LHG-8L (●) and LHG-8H (○), respectively. The data are for (a) 25°C and (b) 150°C. The curves are model calculations using Eq. (7) and the model parameters listed in Table 2. The smooth dashed curves are drawn through the points representing region III growth (the model does not treat region III).

the stress-enhanced reaction between  $H_2O$  and P–O–P or P–O–M at the crack tip. Hillig and Charles [12] and later Wiederhorn [6,31] have described the crack velocity in region I by a reaction rate expression

$$v_I = A \left( \frac{p}{p_0} \right)^m \exp \left( \frac{K_I b - Q_I}{RT} \right), \quad (3)$$

where  $v_I$  is the crack velocity in region I (m/s),  $A$  a pre-exponential constant (m/s),  $p$  the water vapor pressure (mmHg),  $p_0$  the atmospheric pressure (760 mmHg),  $b$  a parameter ( $m^{5/2}/mol$ ) related to activation volume and radius of curvature of the crack tip,  $Q_I$  the activation energy (kJ/mol), and  $m$  is the ‘order’ of the reaction that often appears in reaction rate expressions. In our previous study [14] the above model described crack growth in LG-770 over the whole range of experimental conditions except in regions where crack blunting or capillary condensation occurred. The model uses a single set of fitting parameters:  $A$ ,  $m$ ,  $b$  and  $Q_I$ . The same model analysis that was done for LG-770 samples has also been carried out in this study for LHG-8L and 8H samples (see Section 4.3). The only exception is that  $m$  is fixed at 1.2 as determined for LG-770. Setting  $m$  equal to 1.2 assumes the reaction is nearly first-order in terms of the water vapor concentration; similar first-order reactions have been reported for other glasses, particularly silicates [6,31]. The magnitudes of the other three model parameters determined for the two LHG-8 glasses are summarized in Table 2.

The crack velocity in region II is constant at about  $10^{-5}$  m/s at 25°C and a water vapor pressure of 2 mmHg (see Fig. 3(a)). In this region crack propagation is limited by the mass transport of  $H_2O$  to the crack tip; given in terms of the flux, this is then

$$v_{II} \propto D \frac{\partial C_{H_2O}}{\partial z}, \quad (4)$$

where  $D$  is the  $H_2O$  diffusion coefficient and  $\partial C_{H_2O}/\partial z$  is the concentration gradient in the direction,  $z$ , of crack propagation. Based on Eq. (4),

Table 2

Model parameters for predicting slow crack growth in LHG-8L and -8H in regions I and II in the absence of crack-tip blunting

Parameter	Units	LHG-8L (128 ppmw OH <sup>a</sup> )	LHG-8H (773 ppmw OH <sup>a</sup> )
$A$	$10^6$ m/s	7.3	7.3
$m$	unitless	1.20	1.20
$Q_I$	kJ/mol	253	239
$b$	J/(mol K)	0.480	0.480
$C$	m/s	180	180
$Q_d$	KJ/mol	26	26

<sup>a</sup> Assumes 30 ppmw OH per  $cm^{-1}$  absorption at  $3000\text{ cm}^{-1}$ .

the rate of crack growth should increase linearly with water vapor concentration (i.e., pressure) provided the diffusion constant is not concentration independent. The exact diffusion mechanism for H<sub>2</sub>O transport to the crack tip is not well-known and could be either via gas phase, surface, and/or Knudsen (capillary) diffusion; all have been proposed at one time or another as the limiting diffusion mechanism for crack growth [13,14]. Determination of the mass transport mechanism is not attempted in this study. Therefore we simply note that the crack growth velocity is proportional to the water vapor pressure and best described by Wiederhorn's mechanism [4]

$$v_{II} = C'(T) \frac{p_{H_2O}}{p_0}, \quad (5)$$

where  $C'(T)$  is temperature dependent and has units of m/s and  $p_0$  is a pressure normalization factor (760 mmHg).  $C'(T)$  contains the temperature dependence of the diffusion constant which is assumed to have an Arrhenius dependence

$$C'(T) = C \exp \frac{Q_{II}}{RT}, \quad (6)$$

where  $C$  is a constant (m/s) and  $Q_{II}$  is the activation energy for H<sub>2</sub>O diffusion (kJ/mol). In the present work, region II was only observed at one experimental condition making it impossible to determine the activation energy,  $Q_{II}$ . Therefore, because of the similar glass composition of LG-770 and LHG-8, we assume that the activation energy for H<sub>2</sub>O transport for both glasses is about the same and use 26 kJ/mol reported previously for LG-770 [14]. Thus, the  $C$  in Eq. (6) is 180 m/s based on the fit to the data.

The crack velocity expressions for region I (Eq. (3)) and region II (Eq. (5)) can be combined into a single expression given by the harmonic mean of  $v_I$  and  $v_{II}$

$$v = \frac{v_I v_{II}}{v_I + v_{II}}, \quad (7)$$

where  $v$  is a 'composite' velocity that in the limit of region I ( $v_I \ll v_{II}$ ) approaches  $v_I$  and in the limit of region II ( $v_{II} \ll v_I$ ) approaches  $v_{II}$ . In addition, it provides a smooth function for describing the transition between the two regions.

In Fig. 3, the composite velocities predicted using Eq. (7) (with the parameters listed in Table 2) are compared to the experimental data. The solid curves represent model prediction. In general the model agrees with the data within  $\pm 10\%$  at the temperatures and water vapor pressures shown (see Fig. 3). Considering that crack velocities vary by four orders of magnitude, the agreement between the model and the data is quite good. Therefore this model can be utilized to predict crack velocities and failure times in LHG-8 laser glass under various loads and environmental conditions. The one caveat is that, as presented, the model is only valid in regions where crack tip blunting is negligible and capillary condensation does not occur; the impact of these phenomena are discussed in Sections 4.4 and 4.5.

#### 4.2. Comparison with crack growth in silicate glasses

Comparison of the model parameters describing crack growth in region I (i.e.,  $Q_I$  and  $b$ ) of different glasses provides some insights into the relationship between crack growth and glass structure (Table 3). First notice that the activation energy for fracture propagation in meta-phosphate glasses (216–253 kJ/mol) is less than for silicates (275–705 kJ/mol). This difference is not surprising considering the smaller fracture toughness and the smaller resistance to crack growth in meta-phosphate as compared to those of silicate glasses [14]. Silica-based glasses have a larger cross-link density (mainly Q<sup>3</sup> and Q<sup>4</sup> species), whereas meta-phosphates are comprised mainly of phosphate chains and rings (mainly Q<sup>2</sup> species) and have fewer cross-links [32]. Decreasing the cross-link density decreases the number of covalent bonds to be broken during crack front propagation. Hence for a fixed energy input we expect cracks to grow further in metaphosphate than in silicate glasses.

There are other data that are consistent with the proposed connection between cross-link density and fracture toughness in phosphate glasses. We have observed that the fracture toughness decreases linearly with an increase in the  $O/P$  ratio

Table 3

Comparison of model parameters describing region I slow crack growth in different glasses in the presence of water vapor

Glass	$Q_1$ (kJ/mol)	$b$ (m <sup>5/2</sup> /mol)	Activation volume <sup>a</sup> (10 <sup>-6</sup> m <sup>3</sup> /mol)	Refs.
61% Lead silicate	348	0.510	52	[45]
Aluminosilicate	705	0.770	79	[45]
Borosilicate crown	275	0.260	27	[45]
Soda-lime silicate	605	0.880	90	[45]
Phosphate (LG-770)	216	0.496	51	[14]
Phosphate (LHG-8L)	253	0.480	49	This study
Phosphate (LHG-8H)	240	0.480	49	This study

<sup>a</sup> Calculated from Eq. (8) assuming a crack tip radius of 1.5 nm.

in a series of phosphate glasses [3]. The structure of phosphate glasses is determined in part by the *O/P* ratio and the cross-link density and chain length decrease with increase in the *O/P* ratio [33,34].

The second model parameter which we compare between glasses is  $b$  (Table 3). Both Wiederhorn and Bolz [5] and Hillig and Charles [12] showed that the parameter,  $b$ , is related to the crack tip radius ( $\rho$ ) and the activation volume for fracture propagation ( $V_a$ )

$$b = \frac{2V_a}{3\sqrt{\pi\rho}} \quad (8)$$

The activation volume [35] can be thought of as the increase in volume of the transition-state in the stress corrosion reaction.  $V_a$  can be estimated from the measured  $b = 0.480$  m<sup>5/2</sup>/mol for LHG-8 if the crack tip radius is known. Here we assume a crack tip radius of 1.5 nm based on work of Bando et al. [36]; the calculated activation volume via Eq. (8) is  $49 \times 10^{-6}$  m<sup>3</sup>/mol. Repeating the calculation for the other glasses in Table 3 gives activation volumes ranging from  $49$  to  $90 \times 10^{-6}$  m<sup>3</sup>/mol. The activation volume computed for LHG-8 corresponds to a characteristic length of 0.44 nm, 50% longer than the P–O–P bond length of 0.302 nm. A volume increase in the activated state on the order of the bond length is not unreasonable; bimolecular reactions typically have activation volumes that correspond to 10–100% increase in the bond length [35]. However we must be cautious of a strict physical interpretation of this volume because it depends on the crack tip radius assumed in the calculation.

#### 4.3. Effect of OH content in glass

The introduction of OH into the glass structure is known to affect a number of properties of both silicate [20] and phosphate [37] glasses. In particular, the glass transition temperature and the viscosity both decrease with increase in OH content. For example, in the case of LHG-8, an increase in OH content from 128 to 773 ppmw results in a decrease in  $T_g$  from 472°C to 425°C (see Table 1).

As described in Section 3, increase in the –OH content in the glass increases crack growth velocities in regions I and III (see Fig. 4). We suggest that the crack growth results indicate an increase in the OH content of the glass decreases the overall strength (i.e., fracture resistance). Therefore, it is not surprising that both region I and III are affected by OH content in the glass; in region I crack growth is determined by the rate of the stress corrosion reaction and in region III the on-set of growth is determined by the glass fracture toughness. In contrast, the crack growth in region II is limited by H<sub>2</sub>O transport to the crack tip and thus the ‘plateau’ velocity is not expected to depend on glass OH content. Nevertheless, the onset of region II growth should be dependent on the glass OH content simply because of the shift in the region I (and III) velocities to a smaller  $K_I$ . This shift is shown in Fig. 4(a).

We propose that the observed increase in crack propagation velocities due to larger OH content are related to modification of the phosphate glass structure. The basic structure of phosphate glasses has been well studied and it is known [33] that near meta-phosphate glasses, such as LHG-8, can be structurally described as phosphate chains [34]

(analogous to linear polymeric materials) with a repeating structural unit



where M schematically represents the modifier cation and  $m$  represents the number of structural units in a chain. During melting and forming,  $\text{H}_2\text{O}$  from the atmosphere and from the raw materials are assumed to react with the glass structure by the reaction shown in Eq. (1a) [38]. The addition of OH reduces the average molecular weight of the phosphate chains. This reduction correlates with the observed decrease in viscosity and glass transition temperature. This same effect is observed in most linear polymers (i.e., as the average chain length decreases so does the  $T_g$  and viscosity) [39]. Several studies have shown that addition of OH to the structure of phosphate and silicate glasses reduces chain lengths and/or cross-link densities in the glass [20,34,38].

The effects of different chain lengths (i.e., average molecular weights) on the slow crack growth velocities in linear organic polymers has been reported by several authors [24–29]. In all these studies the slow crack growth velocity was observed to increase with a decrease in the polymer mean molecular weight, similar to that observed here for the LHG-8 samples. Although most organic polymers undergo plastic deformation while glasses undergo ‘brittle’ fracture, some of their similarities can provide insight to the effect of OH content on glass structure and crack growth. Huang and Brown [25] measured crack velocities in polyethylene of different molecular weights and proposed that molecular weight reduction decreased the number of ‘tie’ molecules at the crack tip zone and thereby affected the crack velocity. A ‘tie’ molecule is one that bridges the walls of the crack near the tip. Similarly, Michel et al. [26] report the affects of polymer molecular weight on crack growth in PVC and PMMA and relate this

to a change in the number of chain entanglements (per unit area) in the stressed region of the crack tip.

Assuming an ‘ideal’ meta-phosphate glass ( $O/P = 3$ ) with infinitely long chains, then the effect of added OH on the average ‘molecular weight’ (i.e., chain length) of LHG-8 glass can be estimated as

$$\text{MW}_{\text{glass}} = \frac{3.4 \times 10^7 (\text{gm/mol}) / \text{ppmw}}{[\text{OH}]}, \quad (10)$$

where [OH] is the OH concentration in ppmw and the constant ( $3.4 \times 10^7$ ) represents the molecular weight for a glass with 1 ppmw OH assuming all the OH molecules act as chain-terminating species. From Eq. (10) the average molecular weight of LHG-8L is  $26 \times 10^4$  gm/mol (at 128 ppmw OH) and of LHG-8H is  $4.3 \times 10^4$  gm/mol (at 773 ppmw OH). The difference in the region I crack velocity caused by this change in molecular weight is about 60-fold based on using the crack growth data at 25°C and 2 mmHg water vapor pressure (Fig. 4(a)). Using crack growth data taken under similar conditions for PMMA [25], 30-fold increase is observed. Note that the crack velocities are smaller at larger molecular weights. We suggest that the similarities between the effects of molecular weight on measured crack velocities in meta-phosphate glass and linear organic polymers indicate a similarity in fracture mechanism. In particular, an increase in the OH content in the glass likely decreases the number of bonds per unit area to be broken during fracture (i.e., the covalent P–O–P bonds). Consequently, the activation energy required for fracture ( $Q_1$ ) should also decrease.

We used the same reaction rate model discussed in Section 4.1 to fit the data for the greater OH containing glass, LHG-8H. However, we kept all the model parameters equal to those determined for LHG-8L except the activation energy for region I crack growth,  $Q_1$ . We reasoned that the change in OH content should only affect the energy associated with the bond breaking process during fracture and therefore only affect  $Q_1$ . We suggest that the agreement between the model predictions and the data indicate that this assumption is valid. The  $Q_1$  determined from a fit to the data for the LHG-8H glass is  $239 \pm 3$  kJ/mol

and, as expected, is less than the value for LHG-8L sample ( $253 \pm 3$  kJ/mol). The crack growth is very sensitive to the activation energy and thus the error limits, as reported above, are small. These limits were determined by fitting Eq. (7) to the upper and lower error bars of the data shown in Fig. 4.

In the remainder of this section, a simple model is described to quantify the relationship between  $Q_1$  and the glass OH content. This model is governed by the following assumptions: (1) the addition of OH to the glass reduces the number of P–O–P linkages in the structure; (2) the rate of crack propagation is dominated in part by cleavage of the covalent P–O–P bonds (see discussion in introduction); and (3) the activation energy for fracture ( $Q_1$ ) is proportional to the energy required for bond breaking. Note that assumption 2 implies the cation-to-oxygen bond energies are greater for P–O bonds than for the modifiers. This implication is indeed the case for all the modifiers except  $Al^{3+}$ . In the case of Al (four-fold coordination) the bond energy is approximately equivalent to that for the P–O bond [40].

Consider a plane running through an unfractured glass; it contains a surface density of  $n$  P–O–P bonds per unit area that must be broken when a crack propagates along that surface. Thus, the energy,  $Q_1$ , required for fracture is assumed to be proportional to the areal density of P–O–P bonds ( $n$ )

$$Q_1 = \frac{n}{n_0} E_0, \quad (11)$$

where, in the absence of glass,  $n_0$  is the areal density of P–O–P bonds (hereafter simply called the ‘bond density’) and  $E_0$  is the fracture activation energy. As discussed above, the P–O–P bond density decreases as the OH concentration increases.

The quantity,  $n_0$ , is related to the glass molar volume,  $V_m$ , ( $m^3/mol$ ) by

$$n_0 = \left( \frac{N_A}{V_m S} \right)^{2/3}, \quad (12)$$

where  $N_A$  is Avogadro’s number and  $S$  is the number of atoms in a ‘monomer’ of the phosphate chain (Eq. (9)). We relate the OH concentration to

the areal density of OH bonds using a simple 2/3 power volume-to-area scaling relationship

$$n_{OH} = \left( \frac{[OH] \rho_{gl} N_A}{MW_{OH}} \right)^{2/3}, \quad (13)$$

where  $n_{OH} = n_0 - n$ ,  $\rho_{gl}$  is the density of the glass ( $g/cm^3$ ) and  $MW_{OH}$  is the hydroxyl group molecular weight ( $g/mol$ ). Substituting Eqs. (12) and (13) into Eq. (11), gives an expression that describes the activation energy of fracture as a function of –OH content in the glass

$$Q_1([OH]) = \left( \frac{(N_A/(V_m S))^{2/3} - ([OH] \rho_{gl} N_A / MW_{OH})^{2/3}}{(N_A/(V_m S))^{2/3}} \right) E_0, \quad (14)$$

where for LHG-8,  $V_m$  is  $39 \text{ cm}^3/mol$ ,  $\rho_{gl}$  is  $2.83 \text{ g/cm}^3$  and  $S$  is 5.

The activation energies determined from the reaction rate model, fit to the measured crack growth velocities for LHG-8L and 8H, can be compared to the activation energy predicted by Eq. (14). Based on the  $Q_1$  for LHG-8L ( $253 \pm 3$  kJ/mol) and its hydroxyl content (128 ppmw), the activation energy,  $E_0$ , for fracture growth in a hydroxyl-free glasses is computed to be  $260 \pm 3$  kJ/mol using Eq. (14). Using this  $E_0$ , the calculated  $Q_1$  for LHG-8H (773 ppmw) is  $238 \pm 3$  kJ/mol. This energy is in agreement with the energy obtained by fitting the reaction rate model (Eq. (7)) to the slow crack growth data ( $Q_1 = 239 \pm 3$  kJ/mol, see Table 2).

A simple physical representation of the effect of OH content on the number P–O–P bonds to be broken on a fracture surface is given in Fig. 5. A hypothetical glass sample under tensile load and containing a pre-existing fracture is pictured at the bottom of Fig. 5. Also shown is a  $15 \times 15 \text{ nm}^2$  plane extending beyond the crack front plane, into the unfractured glass. The expected OH density in this plane, for both LHG-8L and 8H, is represented by the black dots in the grids in the top portion of Fig. 5. The grid size ( $0.7 \text{ nm} \times 0.7 \text{ nm}$ ) approximates the overall bond density ( $n_0 \cong 2 \text{ nm}^{-2}$  from Eq. (12)), and the number of hydroxyl groups within each  $15 \times 15 \text{ nm}^2$  surface is

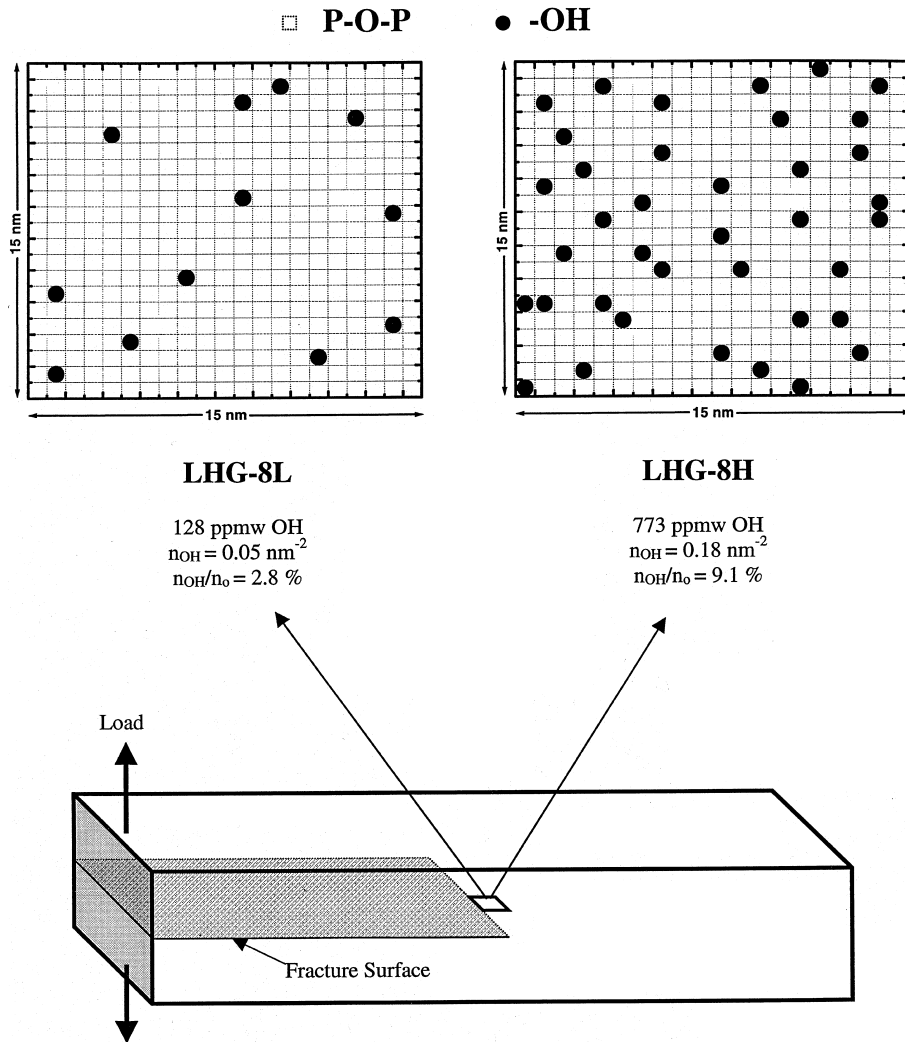


Fig. 5. Hypothetical representation of a glass sample undergoing brittle-fracture illustrating how a change in -OH content in the glass would alter the number of bonds to be broken as the crack propagates. The grid represents a cross-section of the potential fracture surface for both a low (LHG-8L) and high (LHG-8H) OH containing glass. Each square in the grid represents (on average) a bonding site, and each circle represents a bonding site on the fracture surface that has been broken due to a chain terminating OH group.

calculated using Eq. (13). Based on this simple picture, the increase in the OH content in going from LHG-8L to 8H reduces the P-O-P bond density across the fracture plane by about 7%, in agreement with the  $\sim 6\%$  change in activation energy ( $Q_1$ ) for crack growth in these two glasses. Note that this ability to measure small relative changes in activation energy is due to the sensitivity of the crack velocity to small changes in

activation energy. For example, a change of 14 kJ/mol in activation energy governing crack growth (i.e., from 239 to 253 kJ/mol) produces a change in the crack velocity by a factor of 100 (see Fig. 4).

#### 4.4. Crack blunting

Due to the geometry of the DCDC crack growth method (Fig. 1), the stress intensity

decreases with increase in crack length (Eq. (2)); hence the crack velocity decreases over the course of the test. We observed that under conditions of relatively low temperatures and water vapor pressures, the crack velocity decreases; when the crack movement becomes undetectable, a small increase in load (<40 N (~10 lbf)) restarts crack propagation. However, at higher temperatures and water vapor pressures, we found that the propagating crack often stops abruptly. Furthermore, an increase in load, typically >400 N (~ 100 lbf), is required to restart crack growth, and once restarted the crack propagates at greater velocity, in many cases much greater than can be measured by our apparatus. We refer to this arrest in crack propagation as crack tip blunting where the term ‘blunting’ infers an increase in radius of curvature of the crack tip. The effect of crack tip radius ( $\rho$ ) on the local stress at the crack tip ( $\sigma_{\max}$ ) was first formulated by Inglis [41]

$$\sigma_{\max} \propto \frac{1}{\sqrt{\rho}}. \quad (15)$$

As the radius of curvature increases, the local stress at the crack tip decreases. This decrease in the local stress reduces the rate of crack propagation.

The conditions where blunting was observed during the course of this study are shown in Fig. 6. For comparison, also shown, is the complete range of conditions for which crack growth measurements were made. The edge of the shaded region represents the approximate transition from blunting to non-blunting conditions and compares well with the transition zone we observed in previous work [14].

We assume that the blunting process is the result of mass transport of glass to the crack tip; this is conceptually similar to the material transport that occurs during sintering of small particles [42]. A number of mass transport mechanisms are possible including viscous flow, evaporation–condensation, surface diffusion and bulk diffusion. Viscous flow near the crack tip is perhaps the most likely mass transport mechanism because of the decrease in phosphate glass viscosity with increasing hydroxyl content. Therefore at higher

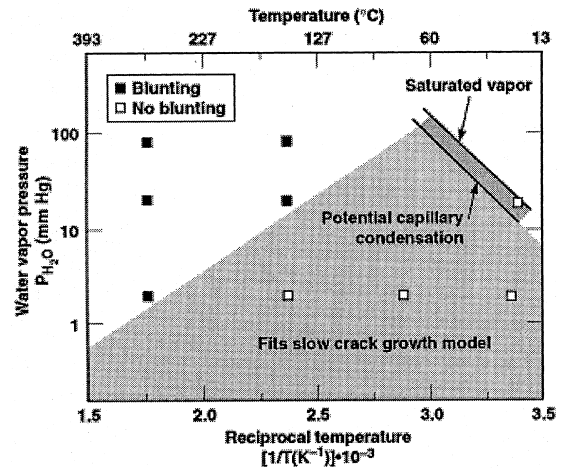


Fig. 6. Conditions (temperature and water vapor pressure), represented by the points, for which crack propagation measurements were made during the course of this work. Also shown are the regions where crack tip blunting was observed and the region for possible capillary condensation. The boundary separating the various regions is approximate.

temperatures and greater water vapor pressures, where OH diffusion into the glass surrounding the tip becomes more rapid, we expect to see a greater degree of blunting. This expectation agrees with our general observations (Fig. 6).

Up to this point, crack blunting (static blunting) is simply described as a decrease in the crack tip curvature that occurs after the crack has stopped. However, the driving force for blunting must also exist even while the crack is propagating; therefore, the propagating crack tip radius could differ depending on the temperature, water vapor pressure and stress intensity (i.e., velocity). We refer to this process as ‘dynamic’ crack tip blunting. Therefore, the size of the crack tip radius is determined by a balance between the rate of mass transport to the crack tip (leading to blunting) and the rate of crack propagation (leading to crack sharpening). In a moving crack, we expect a constant radius of curvature that can be described by

$$\rho = \rho_0 + \rho_b([\text{OH}], T, p, v), \quad (16)$$

where  $\rho$  is the observed radius of curvature,  $\rho_0$  the atomically sharp crack tip, and  $\rho_b$  is the contribution of mass transfer to the crack tip radius. In the case of crack propagation in an ideal brittle

material, the observed crack tip radius is equal to  $\rho_0$  and is expected to be on the order of a bond length ( $\sim 0.15$  nm). In a material that is not per-

fectly brittle,  $\rho_b$  contributes to the total crack tip radius. The degree of blunting that takes place is a function of the OH content in the glass, tempera-

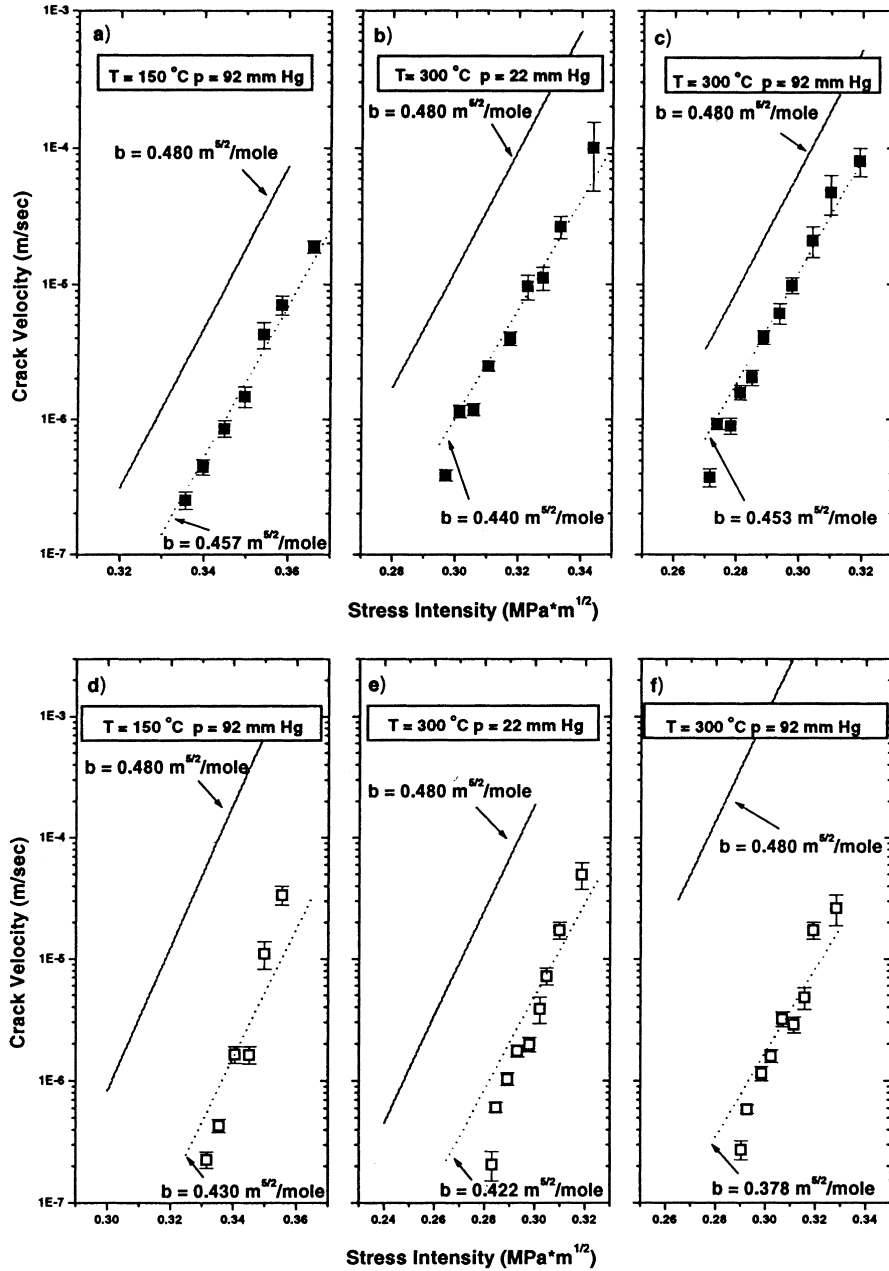


Fig. 7. Measured crack velocities for LHG-8L (a)–(c) and LHG-8H (d)–(f) at temperatures and water vapor pressures where crack-tip blunting was observed. The solid curves represent the predicted dependence using Eq. (3) and assuming no blunting ( $b = 0.480 \text{ m}^{5/2}/\text{mol}$ ). The dash curves represent the predicted dependence using Eq. (3) but varying  $b$  to account for crack tip blunting.

ture, water vapor pressure, and, of course, the velocity of crack propagation (i.e.,  $K_I$ ). Note that crack blunting which occurs once the crack stops ('static' blunting) is simply a limiting case for the above conceptual model.

In instances where blunting is experimentally observed, the region I slow crack growth model (Eq. (3)) does not predict the crack velocity. Differences between model predictions of crack velocities and measured velocities in the blunting region are illustrated in Fig. 7(a)–(c). The solid curves in Fig. 7 represent crack velocities predicted by the region I reaction rate model using the parameters in Table 2. The crack velocity predicted using Eq. (3) is dependent on the crack tip radius through the constant  $b$ ; based on Eq. (8),  $b$  is proportional to  $\rho^{-1/2}$ . Note that because of the exponential dependence of  $v_I$  on  $b$ , the velocity is affected by small changes in crack tip radius,  $\rho$ ; a 10% increase in the radius of curvature typically causes 10-fold reduction in the crack velocity.

The  $b$  determined in the region of negligible blunting is  $0.480 \text{ m}^{5/2}/\text{mol}$  and it predicts crack growth velocities in that region (see Fig. 6). However, using this  $b$  the predicted crack velocity under blunting conditions does not agree with the data as shown in Fig. 7. The reduction in  $b$  (while holding all other model parameters constant) needed to obtain a fit to the data corresponds to about a 12% increase in the crack tip radius for these temperatures and water vapor pressures (see dashed lines in Fig. 7). This increase in crack tip radius agrees with that reported from crack growth measurements on another phosphate glass under similar conditions [14].

In the glass containing the greater OH content (LHG-8H), blunting under the same experimental conditions as LHG-8L (see Fig. 6) was observed. A similar analysis of dynamic blunting was carried out on this glass and the results are shown in Fig. 7(d)–(f). Again the solid curves represent predicted crack velocities using Eq. (3) and Table 2 parameters, and the dashed lines are the best fits obtained by adjusting  $b$ . A larger adjustment in  $b$  (corresponding to a radius of curvature change of between 25 and 60%) was required for the greater OH content of the glass, the more prone it is to

blunting. Fig. 8 further illustrates this effect. Here the ratios of the LHG-8H/LHG-8L crack velocities (at the same stress intensity) are plotted as a function of water vapor pressure. At water vapor pressures of 2 mmHg, the OH content of the glass dominates the crack growth; notice that the velocities are approximately 30 times greater in the sample with the larger amount of OH. On the other hand, at higher humidity (92 mmHg) the LHG-8H sample has velocities only about three times greater than the LHG-8L sample. The much greater relative decrease in crack velocities observed in the high OH glass with increased vapor pressure indicates that this glass is more susceptible to blunting.

#### 4.5. Water condensation at crack tip

At  $25^\circ\text{C}$  and 22 mmHg  $\text{H}_2\text{O}$ , the measured crack velocities for both LHG-8L and H samples did not follow the expected temperature or  $K_I$  dependence (see Fig. 9). The measured crack growth under these conditions may be affected by capillary condensation of liquid water at the crack tip as suggested by Crichton et al. [14]. Crack growth velocities are greater in liquid water compared to water vapor [5]. At  $25^\circ\text{C}$  the saturated vapor pressure for water is only 23.7 mmHg. Hence a water vapor pressure of 22 mmHg at  $25^\circ\text{C}$

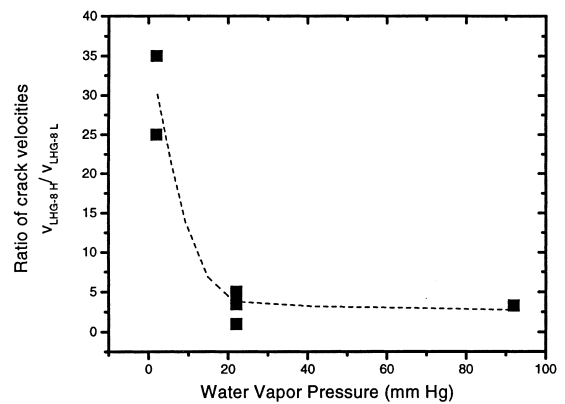


Fig. 8. Ratio of measured crack velocities in LHG-8H (128 ppmw –OH) to that in LHG-8L (773 ppmw –OH) as a function of water vapor pressure. Data are for a fixed  $K_I$ . The line is drawn as a guide for the eye.

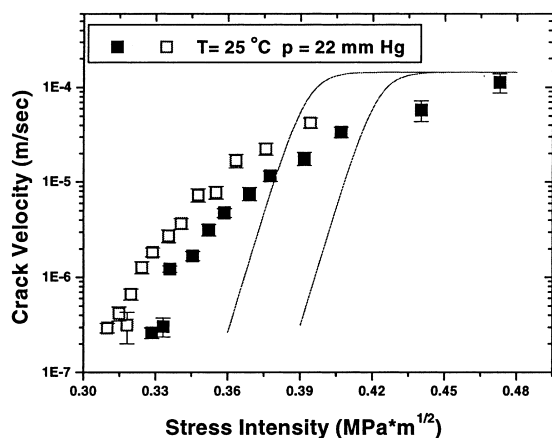


Fig. 9. Crack velocities for LHG-8L (■) and LHG-8H (□) measured at 25°C and 22 mm Hg. The solid curves represent the predicted crack velocities based on the Wiederhorn model for region I and II crack growth (Eq. (7)).

is close to the dewpoint. Therefore liquid water may form at the crack tip due to temperature variations within the apparatus. In addition, the curved surface at crack tip can lead to capillary condensation as predicted by the well-known Kelvin equation [43]. The region of expected capillary condensation (for a crack tip radius of 1.5 nm) is shown in Fig. 6. Note the condition where increased slow crack growth is observed also falls within this region. Measurements under similar conditions on another metaphosphate glass showed the same effect [14].

Apart from the increased crack growth velocities, the data at 25°C and 22 mmHg H<sub>2</sub>O also depart from the expected linear dependence of  $\log v$  with  $K_I$  (Fig. 9). The curvature in these plots is similar to that seen in data on other glasses measured in liquid water and saturated water vapor environments [31,44].

## 5. Conclusions

The crack velocities for both LHG-8 samples in regions I and II can be described using Wiederhorn's chemical and mass transport limited reaction rate model for crack growth. The model is fit to the data using a single set of parameters that

predict crack velocities as a function of temperature, water vapor pressure and stress intensity in the absence of crack blunting and capillary water condensation at the crack front.

An increase in OH content of the glass results in an increase in the slow crack growth velocities in region I and III. We argue that the greater velocities in regions I and III are due to a strength decrease which we attribute to a reduction in the number of P–O–P bonds at the fracture surface caused by chain terminating P–OH. A simple model relates the glass OH content to the activation energy for fracture. The activation energies predicted from this analysis correlate with the activation energies obtained by fitting the reaction rate model to the measured crack velocities.

At higher temperatures and water vapor pressures, crack blunting is observed. Under these conditions measured crack velocities are less than those predicted using the reaction rate expression. An increase in the crack tip radius can account for these discrepancies. We propose that the steady-state crack tip radius is determined by a balance between the rate of mass transport (causing blunting) and the rate of crack propagation (causing crack sharpening). The higher –OH content glass is found to be more susceptible to blunting.

## Acknowledgements

The assistance of Ms Andrea Flammini and Ms Alene Clasen in the preparation of this manuscript and the contributions by the late W.A. Steele for designing and fabricating the experimental setup are deeply appreciated. This work was supported by the US Department of Energy by Lawrence Livermore National Laboratory under contract No. W-7405-ENG-48.

## References

- [1] B.M. VanWanterghem, J.R. Murray, J.H. Campbell, D.R. Speck, C.E. Barker, I.C. Smith, D.F. Browning, W.C. Behrendt, Appl. Opt. 36 (1997) 4932.
- [2] J.T. Hunt, D.R. Speck, Opt. Eng. 28 (1989) 461.

- [3] J. Campbell, T. Suratwala, J. Non-Cryst. Solids (1999) these Proceedings.
- [4] S. Wiederhorn, J. Am. Ceram. Soc. 50 (1967) 407.
- [5] S. Wiederhorn, L. Bolz, J. Am. Ceram. Soc. 53 (1970) 543.
- [6] S. Wiederhorn, J. Am. Ceram. Soc. 55 (1972) 81.
- [7] S. Wiederhorn, E.R. Fuller, R. Thomson, Met. Sci. (August–September) (1980) 450.
- [8] M. Tomozawa, W. Han, W. Lanford, J. Am. Ceram. Soc. 74 (1991) 2573.
- [9] M. Tomozawa, Phys. Chem. Glasses 39 (1998) 65.
- [10] T. Michalske, V. Frechette, J. Am. Ceram. Soc. 63 (1980) 603.
- [11] T. Michalske, B. Bunker, J. Am. Ceram. Soc. 76 (1993) 2613.
- [12] W. Hillig, R. Charles, in: V. Zacklay (Ed.), High Strength Materials, Wiley, New York, 1965, p. 682.
- [13] B. Lawn, Mater. Sci. Eng. 13 (1974) 277.
- [14] S. Crichton, M. Tomozawa, J. Hayden, T. Suratwala, J. Campbell, J. Am. Ceram. Soc. 82 (1999) 3097.
- [15] E. Gehrke, Silikattechnik 33 (1992) 238.
- [16] J.R. Murray, ICF Quarterly Report, LLNL Report UCRL-LR-105821-97, 7 (1997) 95.
- [17] M. Andre, M. Novaro, D. Schirmann, Chocs. Rev. Sci. Techni. Direct. Appl. Milit. 13 (1995) 73.
- [18] J. Campbell, T. Suratwala, C. Thorsness, J. Hayden, A. Thorne, J. Cimino, A. Marker, K. Takeuchi, M. Smolley, G. Ficini-Dorn, these Proceedings, p. 342.
- [19] V. Scholze, Glastech. Ber. 32 (1959) 381.
- [20] J. Shelby, Handbook of Gas Diffusion in Solids and Melts, ASM International, Materials Park, OH, 1996, p. 217 (Chapter 10).
- [21] H. Toratani, Properties of laser phosphate glasses, PhD thesis, Kyoto University, 1989.
- [22] T. Michalske, W. Smith, E. Chen, Eng. Fracture Mech. 45 (1993) 637.
- [23] S. Wiederhorn, in: R. Bradt, D. Hasselman, F. Lange (Eds.), Fracture Mechanics of Ceramics, Plenum, New York, vol. 2, 1996, p. 613.
- [24] A. Tobolsky, H. Eyring, J. Chem. Phys. 11 (1943) 125.
- [25] Y.L. Huang, N. Brown, J. Mater. Sci. 23 (1988) 3648.
- [26] J. Michel, J.A. Manson, R.W. Hertzberg, Polymer 25 (1984) 1657.
- [27] S.L. Kim, M. Skibo, J.A. Manson, R.W. Hertzberg, Polym. Eng. Sci. 17 (1977) 194.
- [28] G. Pitman, I.M. Ward, J. Mater. Sci. 15 (1980) 635.
- [29] A. Ramirez, J. Manson, R. Hertzberg, Polym. Eng. Sci. 22 (1982) 975.
- [30] K.P.R. Reddy, E.H. Fontana, J.D. Helfinstine, J. Am. Ceram. Soc. 71 (1988) C310.
- [31] S. Wiederhorn, in: R.C. Brandt, D.P.H. Hasselman, F.F. Lange (Eds.), Fracture Mechanics in Ceramics, Plenum, New York, 1978, p. 549.
- [32] R.J. Kirkpatrick, R.K. Brow, Solid State Nucl. Magn. Reson. 5 (1995) 9.
- [33] S. Martin, Eur. J. Solid State Inorg. Chem. 28 (1991) 163.
- [34] J. Otaigbe, G. Beall, TRIP 4 (11) (1997) 369.
- [35] S.D. Haman, in: R. Bradley (Ed.), High Pressure Physics and Chemistry, 1963 (Chapter 8).
- [36] Y. Bando, S. Ito, M. Tomozawa, J. Am. Ceram. Soc. 67 (1984) C-36,37; C-254.
- [37] J.S. Hayden, A.J. Marker, T. Suratwala, J.H. Campbell, these Proceedings, p. 228.
- [38] R.M. Wenslow, K.T. Mueller, J. Phys. Chem. B 102 (1998) 9033.
- [39] L.H. Sperling, Introduction to Physical Polymer Science, 2nd Ed., Wiley, New York, 1992.
- [40] K. Sun, J. Am. Ceram. Soc. 30 (1947) 277.
- [41] C. Inglis, Trans. R. Inst. Nav. Archit. 60 (1913) 219.
- [42] W.D. Kingery, H.K. Bowen, D.R. Uhlmann, Introduction to Ceramics, 2nd Ed., Wiley, New York, 1976.
- [43] P. Atkins, Physical Chemistry, 5th Ed., Freeman, Oxford, 1994.
- [44] S. Wiederhorn, J. Am. Ceram. Soc. 56 (1973) 192.
- [45] S. Wiederhorn, H. Johnson, A. Diness, A. Heuer, J. Am. Ceram. Soc. 57 (1974) 336.